http://dx.doi.org/10.5012/bkcs.2013.34.3.912

Relationship Between the Structure and the Superconductivity in LaFeAsO

Dongwoon Jung,* Sungwoo Cho, and In-Ja Lee†,*

*Department of Chemistry Wonkwang University, Iksan, Jeonbuk 570-749, Korea. *E-mail: djung@wku.ac.kr*
†Department of Advanced Materials Chemistry, Dongguk University, Gyeongju, Gyeongbuk 780-714, Korea
**E-mail: lij@dongguk.ac.kr*
Received December 13, 2012, Accepted December 27, 2012

The electronic structure of LaFeAsO was analyzed by tight-binding band calculation based upon the normal and shrunk lattices. A strong Fermi surface nesting was found in the normal LaFeAsO, while most of the nesting area was disappeared in the shrunk LaFeAsO. It was found, therefore, high pressure atmosphere is required to become a superconductor for LaFeAsO by suppressing the SDW (spin density wave) state through the disappearance of the Fermi surface nesting.

Key Words : Electronic structure, Oxypnictide, Superconductivity, SDW

Introduction

After the report of a high-T_c superconductivity with T_c = 92 K in $YBa_2Cu_3O_{7-d}$,[1] new families of high-T_c copper-oxide superconducting series $A_mB_2Ca_{n-1}Cu_nO_{2n+m+2}$ (A = Tl, Bi, Hg; B = Ba, Sr; m = 1, 2; n = 1-4) have been found.[2-5] All of these copper-oxide superconductors contain perovskite CuO_2 conducting layers and rock-salt A-O layers as their structural building blocks. The m values are 1 and 2 when these compounds have single and double rock-salt A-O layers, respectively, while the n values define the number of CuO_2 layers in a unit cell. The T_c's of these superconductors ranged from 92 K to 135 K depending upon the A element and the number of CuO_2 layers. Along with the research on the copper-oxide superconductors, extensive research efforts have resulted in discoveries of variable non-cuprate superconductors.[6-8] However, the T_c's of non-Cu-based superconductors have not been raised above 23 K which is the T_c of the classical alloy, Nb_3Ge.[9]

Recently, Kamihara *et al*. reported a new Fe-based oxypnictide superconductor, LaFeAsO, whose T_c is about 27 K when small amount of oxygen was doped with fluorine.[10] This finding triggered extensive study on the iron-based oxypnictide superconductors, and resultantly the T_c's of REFeAsO (RE = rare earth metals, Nd, Sm, Pr, Ce) were very rapidly enhanced to above 50 K when La was substituted with smaller Re elements. It was, therefore, resonable to call these series of materials as the member of another high-T_c family.[11] In spite of the success to exhibit the high T_c, the oxypnictides REFeAsO require at least one condition to become superconducting phases. This is the synthetic route of preparing these materials at high pressure up to 4 GPa, and/or F-substitution for oxygen up to 11 atom %. The high pressure synthetic method directly results in the shrinkage of the crystalline lattice, which means that Fe-As and La-O bonds in REFeAsO become shorter. The substitution method contributes in two ways; one is that the substitution of O^{2-} with F^- is nothing more than adding charge carriers into the compound, and the other is the reduction of lattice size by doping with smaller size ion. Whatever the method is adopted, the lattice shrinkage is occurred. For the undoped REFeAsO synthesized at ambient atmosphere, a spin density wave (SDW) was observed at low temperatures by neutron diffraction studies.[12,13] Ren *et al.* reported that the F-doping at the oxygen site suppressed the SDW ordering, thereby leading to the compound become a superconductor.[11] The oxygen defficient phases, $REFeAsO_{1-d}$ were also reported to become superconductors when they were prepared at high pressure.[14] The shrinkage of the crystalline lattice of these compounds by introducing high pressure up to 4 GPa further enhanced the superconducting transition temperature.[15]

In this presentation, the reason why LaFeAsO exhibits superconductivity only when high pressure is applied, will be analyzed by examining the relationship between the lattice parameters and the electronic properties of LaFeAsO. The electronic property will be analyzed by calculating the electronic structure of this compound.

Structure of LaFeAsO. The quaternary LaFeAsO phase is tetragonal with the space group of P4/nmm. The lattice parameter of this compound at room temperature is a = 4.03552(8) Å and c = 8.7393(2) Å for the undoped samples and a = 4.0320(1) Å and c = 8.7263(3) Å for the 5 atom % F-doped samples.[10] The lattice constants decrease gradually with the concentration of smaller F^- ions for the site of O^{2-} ions. Also the smaller lattice parameters of this compound prepared at high pressure are understandable.

The structure of the LaFeAsO compound is constructed with alternating La-O and As-Fe layers along the crystallographic c-direction, as shown in Figure 1. The La-As and La-Fe distances are 3.38 Å and 3.73 Å, respectively. These rather long distances indicate that it may be difficult to be an electron path along this direction. La-O layer runs along the a- and b-directions with the La-O bond distance of 2.367 Å as illustrated in Figure 2. Each oxygen atom bridges two La atoms along the a-direction and along the b-direction. Each

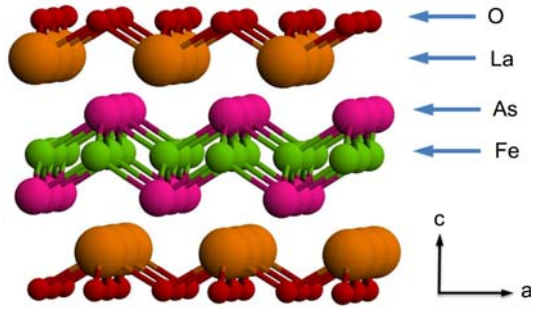

Figure 1. The crystal structure of LaFeAsO.

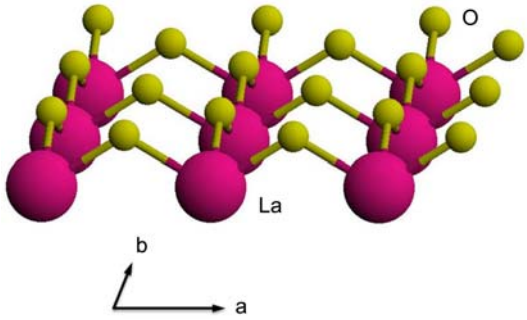

Figure 2. 2-Dimensional La-O slab. Large and small circles represent lanthanum and oxygen atoms, respectively.

La atom is connected to two bridging oxygen atoms along the a-direction, and another two bridging oxygen atoms along the b-direction. In an As-Fe layer, tetrahedrally coordinated $FeAs_4$ units run along the a- and b-directions by sharing their edges as shown in Figure 3. The As-Fe bond distance is 2.412 Å along both directions.

Computational Method. Electronic structure calculations were performed by the extended Hückel method[16] within the framework of tight binding approximation.[17] Density of states (DOS), crystal orbital overlap populations (COOP), and the Fermi surface were calculated based on the given crystal structure of LaFeAsO at room temperature and on the model structure representing the shrunk lattice by 2% from the original room temperature structure. For simplicity, hereafter, the normal and the shrunk structures will be referred to as *n*-LaFeAsO and *s*-LaFeAsO, respectively. The atomic orbital parameters[18-20] employed in the calculation were the default values in the CAESAR program,[21] which are listed in

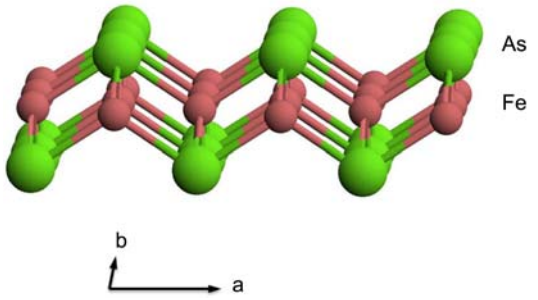

Figure 3. 2-Dimensional As-Fe slab. Large and small circles represent arsenic and iron atoms, respectively.

Table 1. Atomic Parameters used in EHTB Calculations: Valence orbital Ionization Potential H_{ii}(eV) and Exponent of the Slater-type Orbital ζ and the orbital coefficient c

Atom	Orbital	H_{ii}(eV)	ζ_1 (c_1)	ζ_2 (c_2)
As	4s	-16.22	2.23 (1.0)	
	4p	-12.16	1.89 (1.0)	
Fe	4s	-9.10	1.90 (1.0)	
	4p	-5.32	1.90 (1.0)	
	3d	-12.6	5.35 (0.5505)	2.00 (0.6260)
La	6s	-7.67	2.14 (1.0)	
	6p	-5.01	2.08 (1.0)	
	5d	-8.21	3.78 (0.7765)	1.381 (0.4586)
	4f	-5.96	8.35 (0.410)	4.00 (0.730)
O	2s	-32.299	2.275 (1.0)	
	2p	-14.8	2.275 (1.0)	

Table 1. The band structures were calculated along the special lines connecting the following high-symmetry points: G (0,0,0), X (0.5,0,0), Y (0,0.5,0), M (0.5,0.5,0), and R (0.5,0.5,0.5) in terms of the reciprocal basis vectors.[22] Atomic and bond populations were evaluated *via* the Mulliken population analysis.[23] Within the Brillouin zone of the cell, 512 irreducible k points were selected.

Results and Discussion

The total density of states (DOS) and the projected density of states (PDOS) calculated for the La, Fe, As, and O atoms in *n*-LaFeAsO and *s*-LaFeAsO are shown in Figure 4(a) and Figure 4(b). The PDOS of La atoms is not shown for clarity of the figure since the contribution from La atom is almost zero within the calculated energy region. Basically, two data are almost similar so we focus on the analyzation of Figure 4(a) only. The vertical dashed line represents the Fermi energy of the compound. The solid line represents the total DOS of the compound. The dashed, dotted, dash-dot line represents the contribution of Fe, As, and O atoms, respectively. At the Fermi energy, the DOS values for the compound is not zero, which means that *n*-LaFeAsO is metallic. This result is consistent with the experimental data that the resistivity of the compound increases with increasing temperature. Upon the general oxidation scheme of La^{3+}, Fe^{2+}, As^{3-}, and O^{2-}, only Fe^{2+} ions create partially filled bands. The metallic property in this compound is, therefore, arises from the iron ions. The PDOS result is consistent with this expectation. At the Fermi energy, the major contribution to DOS originates from Fe atoms. Although not shown, this Fe contribution comes not from the 4*s*- and 4*p*-orbitals but from the 3*d*-orbitals which means that electrons in Fe 3*d*-orbitals are most important charge carriers. Minor contribution from the As 4*s*- and 4*p*-orbitals is also observed from the PDOS data. The PDOS of O *p*-orbitals contributes totally at −15.8 to −14.4 eV, which is well below the Fermi energy as shown in Figure 4. The major peak for As *p*-orbitals lies in the region of −14.4 to −13.0 eV, meaning that the oxidation state

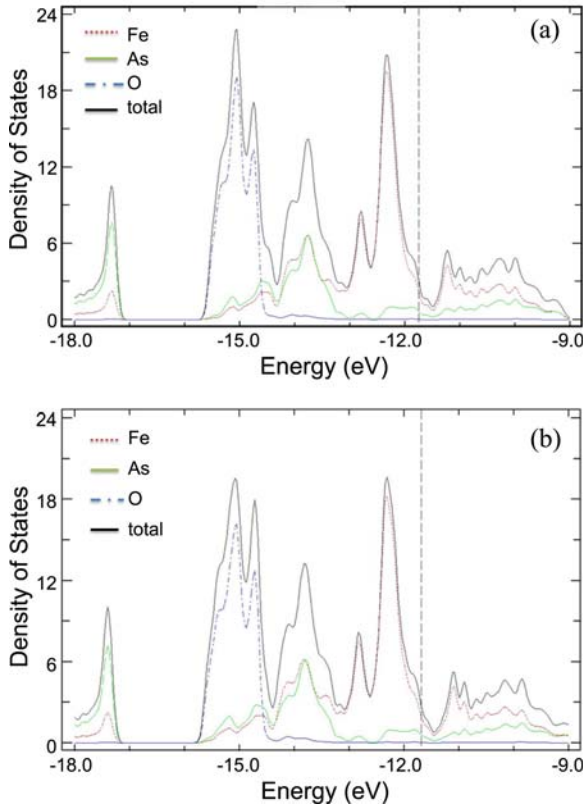

Figure 4. PDOS data calculated for (a) *n*-LaFeAsO and (b) *s*-LaFeAsO. The vertical dashed line represents the Fermi energy.

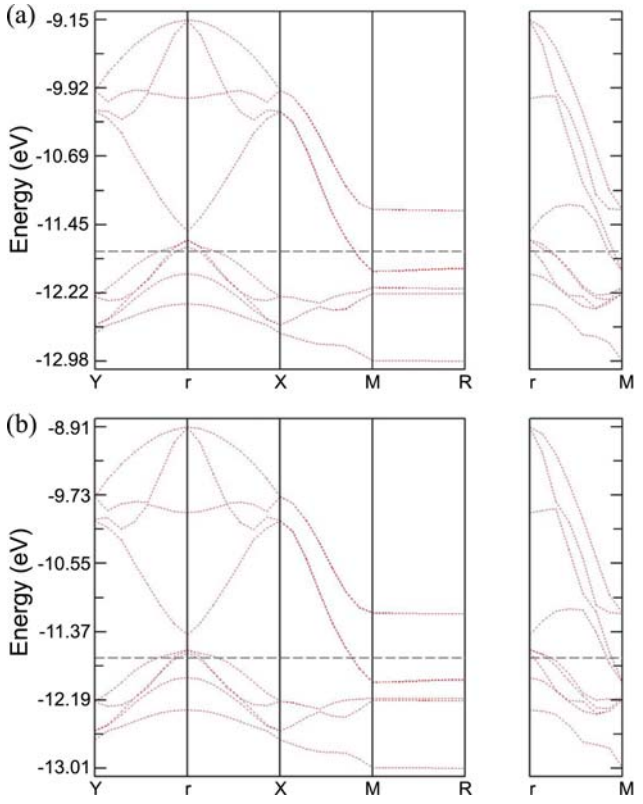

Figure 5. Band dispersion curves calculated for (a) *n*-LaFeAsO and (b) *s*-LaFeAsO around the Fermi energy. The horizontal dashed line represents the Fermi energy.

of As is almost −3. The As-Fe connections along the a- and b-directions are possibly responsible for the conductivity and superconductivity of the LaFeAsO compound.

Band dispersions calculated for *n*-LaFeAsO and *s*-LaFeAsO are shown in Figure 5(a) and Figure 5(b). Likewise to DOS data, two bands are almost similar so the band dispersions for *n*-LaFeAsO are discussed. Only nine bands near the Fermi energy are shown in the figure since the electrons in the bands around the Fermi energy are most important for the electrical conductivity. Five bands out of nine are cut by the Fermi energy. Γ, X, Y, M, R represent the wave vector points (0,0,0), (0.5,0,0), (0,0.5,0), (0.5,0.5,0), and (0.5,0.5,0.5) in the first Brillouin zone of the reciprocal lattice, respectively. From M (0.5,0.5,0) to R (0.5,0.5,0.5) is nothing more than from Γ (0,0,0) to Z (0,0,0.5). Bands are almost flat along the c-direction in LaFeAsO while they are strongly dispersive only along the a- and b-directions, meaning that the orbital interactions occur only along the a-, and b-directions. Band dispersion curve of this compound, therefore, tells us that LaFeAsO is a 2-dimensional metal. This result is consistent with the structural features that LaFeAsO is constructed with alternating La-O and As-Fe slabs which are repeated along the a-, and b-directions. From the PDOS analysis, the major and minor contribution to the conductivity of this compound comes from Fe and As atoms, respectively. The repeating As-Fe tetrahedra, therefore, act as charge carrier paths by forming strong interactions between arsenic and iron atoms along the a- and b-direction (See Figure 1). Structurally, the distances between the La-O and the As-Fe slabs are too long to interact, and electrons cannot move through this c-direction.

The Fermi surface of a partially filled band is defined as the boundary surface of wave vectors that separate the wave vector region of filled band levels from that the wave vector region of unfilled band levels. One piece of a Fermi surface may be superimposable, by translating it with wave vector q, onto an other piece of the Fermi surface. In such a case, the two pieces are said to be nested by the wave vector q. A metallic system with a nesting vector q leads to a Metal-Insulator (M-I) transition. The electronic instability induced by these Fermi surface nestings may cause the charge density waves (CDW) or the spin density waves (SDW) depending upon how their orbitals are mixed.[24,25] Let us discuss why a Fermi surface nesting is important in introducing a phase transition by investigating the orbital mixing between an occupied and unoccupied levels.[26] An occupied wave vector k and a unoccupied wave vector k' form an occupied orbital $\phi(k)$ and a unoccupied orbital $\phi(k')$, respectively. An orbital mixing between $\phi(k)$ and $\phi(k')$ produces new orbitals $\Psi(k)$ and $\Psi(k')$. The extent of the orbital mixing is determined by the energy difference between the original orbitals $\phi(k)$ and $\phi(k')$. At the Fermi level, by definition, two orbitals $\phi(k)$ and $\phi(k')$ are degenerate. Therefore, the orbital mixing between them is significant and so is the interaction energy $<\phi(k)|H'|\phi(k')>$. When a Fermi surface is nested by a vector q, the orbital mixing can be performed for all wave vectors

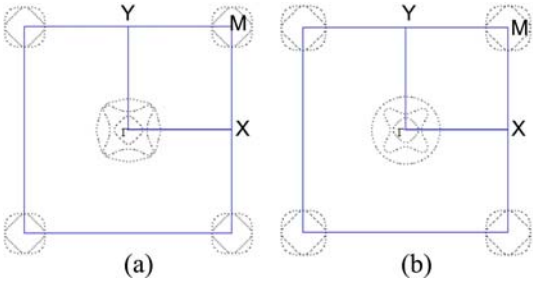

Figure 6. The Fermi surfaces associated with the bands of (a) *n*-LaFeAsO and (b) *s*-LaFeAsO.

in the nested region of the First Brillouin Zone (FBZ). As the nesting area is large, therefore, the amount of orbital mixing is large and so is the extent of interaction energy. This large amount of energy becomes the driving force to change the structure which leads to a M-I transition even at low temperature.

Since five bands are cut by the Fermi energy, five Fermi surfaces can be drawn for *n*-LaFeAsO and *s*-LaFeAsO. The band dispersion data already showed that this compound is 2-dimensional along the a- and b-directions, all Fermi surfaces are drawn in the ab-plane of the reciprocal lattice. Carriers responsible for conductivity of metals are those electrons around the Fermi energy. When a certain wave vector direction cross a Fermi surface (*e.g.*, $\Gamma \rightarrow$ X in Fig. 6(a)), there are electrons at the Fermi level having momentum along that direction, so that the system is metallic along that direction. All Fermi surfaces in Figures 6(a) and 6(b) are closed along the a- and b-directions and there are Fermi surface crossing along those directions. Basically, the Fermi surfaces calculated for two structures are similar in shape. Especially, two Fermi surfaces around M point are almost same as shown in Figures 6(a) and 6(b). However, a striking difference can be found in Fermi surfaces of *n*-LaFeAsO and *s*-LaFeAsO around Γ point. There are three different closed Fermi surfaces around Γ point. Let us call these three Fermi surfaces as square-like, flower-like, and circular shapes from inner to outer direction. The Fermi surface of the square-like shape for *n*-LaFeAsO is well nested with translating vector q_2, while that for *s*-LaFeAsO is changed more circular. If we consider the Fermi surfaces of the flower-like shape for both structures separately, they are same. But the set of Fermi surfaces with the flower-like and circular shape makes quite big difference. Many pieces of the flower-like shape can be superimposed to the pieces of circular shape by translating with wave vector q and q_1 in the Fermi surface of *n*-LaFeAsO, while there is no Fermi surface nesting in that of *s*-LaFeAsO, as illustrated in Figure 7(a), and Figure 7(b). In the long run, the Fermi surface nesting phenomenon disappears when the lattice is shrunk.

In the first cuprate high-T_c superconductor La_2CuO_4, the oxidation state of Cu is exactly 2+, that is, the electron count on copper is d^9. Therefore, the valence band of this system, *i.e.*, the $d_{x^2-y^2}$ band of Cu, is half-filled. The Fermi surface associated with this band has a square shape. The strong Fermi surface nesting induced from this shape causes the

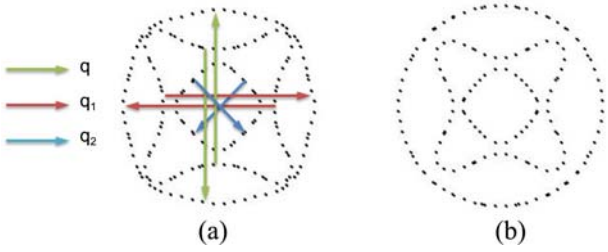

Figure 7. The Fermi surface nesting in (a) *n*-LaFeAsO and (b) *s*-LaFeAsO.

electronic instability in this compound. Consequently, this compound becomes an antiferromagnetic insulator below 533 K.[27] However, when some of the La^{3+} ions are substituted with alkaline earth ions A^{2+} (A = Sr, Ba), the Fermi surface nesting disappears and the resulting material $La_{2-x}A_xCuO_4$ [for which the oxidation state of copper is +(2+x)] becomes a metal and reaches a superconducting state at ~40 K.[28] Likewise, the suppression of the Fermi surface nesting in the shrunk lattice obtained by applying high pressure and/or substituting oxygen ion with smaller fluoride ion, is crucial to become a superconductor for LaFeAsO.

Conclusion

The oxypnictides, REFeAsO (RE = La, Nd, Sm, Pr, Ce) are reported to show relatively high superconducting transition temperature when these materials has shrunk lattices. The reduced lattice can be achieved by applying high pressure atmosphere and/or the substitution of oxygen ion with a smaller fluoride ion. That is, the reduced lattice is inevitable to show the superconductivity in these compounds. The band electronic structure calculation data show that a strong Fermi surface nesting was found in the normal LaFeAsO, while most of the nesting area was disappeared in the shrunk LaFeAsO. It was found, therefore, why high pressure atmosphere is required to become a superconductor for LaFeAsO. This result is consistent with the experimental data that the insulating spin density wave state can be suppressed by applying high pressure on LaFeAsO, or substituting O^{2-} ion with smaller F^- ion to shrink its lattice parameters.

References

1. Wu, M. K.; Ashburn, J. R.; Torng, C. J.; Hor, P. H.; Meng, R. L.; Gao, L.; Huang, Z. J.; Wang, Y. Q.; Chu, C. W. *Phys. Rev. Lett.* **1988**, *58*, 908.
2. Sheng, Z. Z.; Hermann, A. M. *Nature* **1988**, *332*, 138.
3. Sleight, A. W. *Science* **1988**, *242*, 1519.
4. Subramanian, M. A.; Parise, J. B.; Calabrese, J. C.; Torardi, C. C.; Gopalakrishnan, J.; Sleight, A. W. *J. Solid State Chem.* **1988**, *77*, 192.
5. Ihara, H.; Sigise, R.; Hayashi, K.; Terada, N.; Jo, M.; Hirabayashi, M.; Negishi, A.; Atoda, N.; Oyanagi, H.; Shimomura, T.; Ohash, S. *Phys. Rev.* **1988**, *B38*, 11952.
6. Hebard, A. F.; Roseinsky, M. J.; Haddon, R. C.; Murphy, D. W.; Glarum, S. H.; Palstra, T. T. M.; Ramirez, A. P.; Kortan, A. R. *Nature* **1991**, *350*, 660.

7. Nagamatsu, J.; Nakagawa, N.; Muranaka, T.; Zenitani, J.; Akimitsu, J. *Nature* **2001**, *410*, 63.
8. Yonezawa, S.; Muraoka, Y.; Hiroi, Z. *J. Phys. Condens. Matter* **2004**, *16*, L9.
9. (a) Matthias, B. T.; Geballe, T. H.; Longinotti, L. D.; Corenzwit, E.; Hull, G. W.; Matthias, R. H. B. T.; Geballe, T. H.; Longinotti, L. D.; Corenzwit, E.; Hull, G. W.; Williens, R. H.; Maita, J. P. *Science* **1967**, *156*, 645. (b) Gavaler, J. R. *Appl. Phys. Lett.* **1973**, *23*, 480.
10. Kamihara, Y.; Watanabe, T.; Hirano, M.; Hosono, H. *J. Am. Chem. Soc*. **2008**, *130*, 3296.
11. Ren, Z. A.; Yang, J.; Lu, W.; Yi, W.; Shen, X. L.; Li, Z. C.; Che, G. C.; Dong, X. L.; Sun, L. L.; Zhou, F.; Zhao, Z. X. *Europhys. Lett.* **2008**, *82*, 57002.
12. Clarina, de la C.; Huang, Q.; Lynn, J. W.; Li, J. Y.; Ratcliff, W.; Zarestky, J. L.; Mook, H. A.; Chen, G. F.; Luo, J. L.; Wang, N. L.; Dai, P. C. *Cond-mat. arXiv:* **2008**, 0804.0795.
13. McGuire, M. A.; Christianson, A. D.; Sefat, A. S.; Jin, R.; Payzant, E. A.; Sales, B. C.; Lumsden, M. D.; Mandrus, D. *Cond-mat. arXiv*: **2008**, 0804.0796.
14. Ren, Z. A.; Che, G. C.; Dong, X. L.; Yang, J.; Lu, W.; Yi, W.; Shen, X. L.; Li, Z. C.; Sun, L. L.; Zhou, F.; Zhao, Z. X. *Europhys. Lett.* **2008**, *83*, 17002.
15. Takahashi, H.; Igawa, K.; Arii, K.; Kamihara, Y.; Hirano, M.; Hosono, H. *Nature* **2008**, *453*, 376.
16. Hoffmann, R. *J. Chem. Phys*. **1963**, *39*, 1397.
17. Ammeter, J. H.; Bergi, H.-B.; Thibeault, J.; Hoffmann, R. *J. Am. Chem. Soc*. **1978**, *100*, 3686.
18. Clementi, E.; Roetti, C. *Atomic Data Nuclear Data Tables* **1974**, *14*, 177.
19. McLeen, A. D.; McLeen, R. S. *Atomic Data Nuclear Data Tables* **1981**, *26*, 197.
20. Richardson, J. W.; Blackman, M. J.; Ranochak, J. E. *J. Chem. Phys*. **1973**, *58*, 3010.
21. Ren, J.; Liang, W.; Whangbo, M.-H. *CAESAR*; Primecolor Software, Inc.: Cary, NC, 1999.
22. Bradley, C. J.; Cracknell, A. P. *The Mathematical Theory of Symmetry in Solids. Representation Theory for Point Groups and Space Groups*; Clarendon Press: Oxford, 1972.
23. Mulliken, R. S. *J. Chem. Phys*. **1955**, *23*, 1833.
24. Whangbo, M.-H. *J. Chem. Phys.* **1981**, *75*, 4983.
25. Whangbo, M.-H. *J. Chem. Phys.* **1980**, *73*, 3854.
26. Whangbo, M.-H. *Acc. Chem. Res*. **1983**, *16*, 95.
27. Longo, J. M.; Raccah, P. M. *J. Solid State Chem*. **1973**, *6*, 526.
28. Bednorz, J. G.; Muller, K. A. *Z. Phys. B Condensed Matter.* **1986**, *64*, 189.